Knockout Reactions from *p*-Shell Nuclei: Tests of *Ab Initio* Structure Models

G. F. Grinyer,[1,*] D. Bazin,[1] A. Gade,[1,2] J. A. Tostevin,[3] P. Adrich,[1] M. D. Bowen,[1,2] B. A. Brown,[1,2] C. M. Campbell,[1,2] J. M. Cook,[1,2] T. Glasmacher,[1,2] S. McDaniel,[1,2] P. Navrátil,[4,†] A. Obertelli,[1,‡] S. Quaglioni,[4] K. Siwek,[1,2] J. R. Terry,[1,2] D. Weisshaar,[1] and R. B. Wiringa[5]

[1]*National Superconducting Cyclotron Laboratory, Michigan State University, East Lansing, Michigan 48824, USA*
[2]*Department of Physics and Astronomy, Michigan State University, East Lansing, Michigan 48824, USA*
[3]*Department of Physics, University of Surrey, Guildford, Surrey GU2 7XH, United Kingdom*
[4]*Lawrence Livermore National Laboratory, P.O. Box 808, L-414, Livermore, California 94551, USA*
[5]*Physics Division, Argonne National Laboratory, Argonne, Illinois 60439, USA*

(Received 21 December 2010; published 22 April 2011)

Absolute cross sections have been determined following single neutron knockout reactions from ^{10}Be and ^{10}C at intermediate energy. Nucleon density distributions and bound-state wave function overlaps obtained from both variational Monte Carlo (VMC) and no core shell model (NCSM) *ab initio* calculations have been incorporated into the theoretical description of knockout reactions. Comparison to experimental cross sections demonstrates that the VMC approach, with the inclusion of 3-body forces, provides the best overall agreement while the NCSM and conventional shell-model calculations both overpredict the cross sections by 20% to 30% for ^{10}Be and by 40% to 50% for ^{10}C, respectively. This study gains new insight into the importance of 3-body forces and continuum effects in light nuclei and provides a sensitive technique to assess the accuracy of *ab initio* calculations for describing these effects.

DOI: 10.1103/PhysRevLett.106.162502 PACS numbers: 21.10.Jx, 21.60.De, 24.50.+g, 25.10.+s

Describing the structure of finite nuclei from the interactions between individual nucleons is a fundamental goal and outstanding problem in nuclear physics. Practical application of such a ''first principles'' or *ab initio* approach is extremely challenging due in part to the fact that bare nuclear forces are not uniquely defined, solutions to the many-body problem are complicated by both short and long range internucleon correlations, and there is clear evidence that 2-body forces are alone insufficient. Despite these challenges, tremendous progress has been achieved for *p*-shell nuclei with $5 \leq A \leq 16$ through the variational and Green's function Monte Carlo (VMC) [1] and the no-core shell-model (NCSM) [2] techniques. While both of these approaches include realistic 2-body interactions constructed to reproduce a substantial body of free nucleon-nucleon (NN) elastic scattering data, the description of the 3-body ($3N$) forces is much less constrained. In addition to nuclear masses, precise experimental data on matter radii [3], spectroscopic factors [4,5], resonances in unbound systems [6], and electromagnetic transition rates [7] have also been used to quantify the role of $3N$ forces and refine the parameters used in their evaluation. With limited experimental data driving the parametrization of these rapidly developing *ab initio* structure theories, new and precise measurements that probe the structure of *p*-shell nuclei using alternative techniques and providing sensitive benchmarks for theory are essential.

Single nucleon knockout reactions performed at intermediate energy offer an attractive tool to test the predictions of these *ab initio* models. Knockout reactions have their foundations in the study of *p*-shell nuclei, used previously to investigate properties of weakly bound halo nuclei [8–11] and determine spectroscopic factors [12,13]. These reactions have since been extended to heavier mass systems demonstrating sensitivity to single-particle structure for short-lived nuclei available at beam rates of only a few ions per second [14–17]. In the present work, single neutron knockout reactions from radioactive beams of ^{10}Be and ^{10}C were performed to probe the structure of these light nuclei and potentially discriminate between *ab initio* structure model descriptions. Reactions on the ^{10}Be and ^{10}C mirror nuclei form an ideal set for comparison as they cover a broad range in neutron separation energy (6.8 and 21.3 MeV, respectively) and the knockout residues ^{9}C and ^{9}Be have no bound excited states. To provide a consistent theoretical description of the key reaction inputs, point nucleon densities and bound-state wave function overlaps from the fully correlated A-body VMC and NCSM wave functions have been used in the reaction calculations. The results presented here clearly discriminate between the NCSM and VMC theoretical models and provide important and quantitative information necessary for their development.

Beams of ^{10}Be and ^{10}C were produced at the National Superconducting Laboratory's Coupled Cyclotron Facility through projectile fragmentation of a 150 MeV/u beam of ^{16}O incident on a ^{9}Be production target and were separated from additional reaction products using the A1900 fragment separator [18]. Secondary beams with energies of either 80 or 120 MeV/u were then delivered to the experimental area and impinged secondary reaction targets of either 376(4) mg/cm^2 ^{9}Be or 403(5) mg/cm^2 $^{\text{nat}}$C

positioned at the pivot point of the S800 spectrograph [19]. The S800 selected the secondary reaction residue of interest based on magnetic rigidity $B\rho$ and provided an event-by-event particle identification using the focal-plane detection system consisting of two x-y position-sensitive detectors and two plastic scintillators (5 and 10 cm thickness). The scintillators provided both an energy loss (ΔE) and total residue energy (E) measurement in addition to a start signal for the time-of-flight (TOF) measurement. Two thin plastic scintillators (150 μm thickness) were located approximately 25 and 45 m upstream from the secondary target and provided independent TOF stop signals. Inverse ray tracing of the nearly 18 m path from the focal plane of the S800 to the target position was achieved using the ion-optics code COSY [20]. A summary of the experimental parameters is provided in Table I.

Beam rates of order 10^5 ions/s were achieved for both secondary beams. For cross sections of at least 10 mb, data collection over a period of 4 h was sufficient to detect nearly 2.5×10^5 residues. With this statistical precision, uncertainties associated with the experimental cross sections were dominated by systematic losses due to the finite acceptances of the S800 that are limited to $\pm 2.5\%$ in momentum, and $\pm 3.5°$ and $\pm 5.0°$ in the dispersive and nondispersive directions, respectively [15]. Angular acceptance losses were observed to be both mass and energy dependent and required a rigidity dependent correction to be applied to the raw data of order of 10% for the reactions studied. A conservative systematic uncertainty of 5% was then combined in quadrature with the statistical uncertainties. In addition, because the relatively broad momentum distributions of the ^{9}Be and ^{9}C knockout residues exceeded the momentum acceptance of the S800, parallel momentum distributions were constructed in software, as demonstrated in Fig. 1, from data collected at several overlapping magnetic rigidities. The absolute normalization of each data set was achieved independently using data from unreacted beam settings taken between each change of magnetic rigidity. Cross sections were determined from a fit to the parallel momentum distribution that combined the expected shape of the theoretical eikonal distribution [21] with a Gaussian, required to describe low momenta where dissipative stripping events lead to an extended tail [22,23]. A fit function, rather than direct integration, was performed

TABLE I. Summary of reactions, energies, and target materials. Reaction target thicknesses were 376(4) mg/cm^2 and 403(5) mg/cm^2 for the ^{9}Be and ^{nat}C targets, respectively.

Initial state	Final state	Projectile energy (MeV/u)	Secondary target (material)	σ_{exp} (mb)
^{10}Be	^{9}Be	120	Be	73.0(38)
		80	Be	67.5(36)
^{10}C	^{9}C	120	Be	23.2(10)
		120	C	27.4(16)

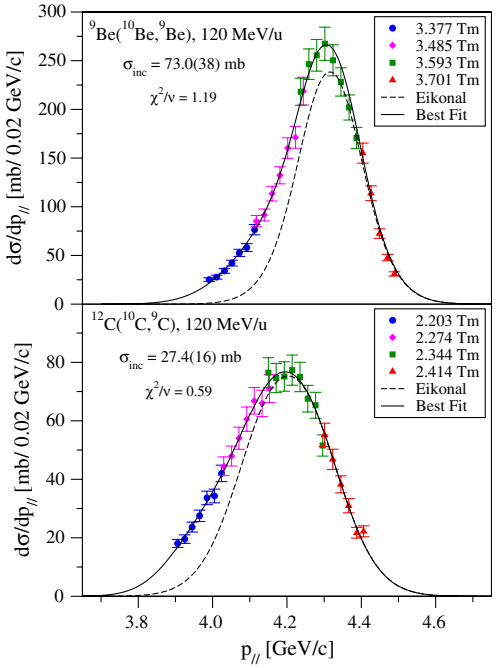

FIG. 1 (color online). Longitudinal momentum distributions for ^{9}Be (top) and ^{9}C (bottom) reaction residues constructed from four overlapping magnetic rigidities. An eikonal-plus-Gaussian fit was employed to estimate the unobserved cross section in the low and high momentum tails.

to provide an accurate estimate for the $\sim 7\%$ of cross section not observed at low and high momenta. Inclusive cross sections σ_{exp} determined in this work are provided in Table I and show only moderate dependence on the incident energy and target material.

Theoretical single-particle cross sections σ_{sp} are calculated using eikonal or Glauber theory [24,25]. In previous studies with heavier projectiles, the residue-target interactions were calculated using point neutron and proton densities of the residue calculated from Hartree-Fock (HF) with Skyrme forces (SkX) [26]. The projectile and residue overlaps were obtained from the shell model, their radial form factors being the eigenstates of a Woods-Saxon-plus-spin-orbit potential with a well depth constrained by experimental separation energies S_n. For a chosen diffuseness a, the radius r parameters were determined from fitting the HF-SkX predictions of the rms radius of the orbital. As discussed in Ref. [16], it is this orbital size parameter that has the most significant impact on the evaluation of the single-particle cross sections and must therefore be consistently specified. Woods-Saxon fit parameters and the single-particle cross sections derived from this approach are listed in Table II and were derived for both projectiles at 120 MeV/u with a ^{9}Be target. Adjusting these inputs to 80 MeV/u or using a ^{nat}C target led to variations in the single-particle cross sections by no more than 2%. The relative insensitivity of the theoretical values to these parameters is consistent with the experimental

TABLE II. Woods-Saxon parameters r, a, and potential depth V_0 for the $\langle {}^{10}\mathrm{Be}|{}^{9}\mathrm{Be}+n\rangle$ and $\langle {}^{10}\mathrm{C}|{}^{9}\mathrm{C}+n\rangle$ overlap fits. Single-particle cross sections σ_{sp} were derived for projectile beam energies of 120 MeV/u on a ^{9}Be target. Spectroscopic factors S_F from each model are used to derive theoretical cross sections σ_{th} and can be compared to the experimental results σ_{exp}.

$\langle {}^{10}\mathrm{Be}\|{}^{9}\mathrm{Be}+n\rangle$	r (fm)	a (fm)	V_0 (MeV)	σ_{sp} (mb)	S_F	σ_{th} (mb)	σ_{exp} (mb)
SM	1.25	0.70	60.4	36.8	2.62	96.6	
NCSM	1.34(2)	0.57(2)	42.9	36.8(7)	2.36	86.9(16)	73(4)
VMC	1.25(3)	0.78(4)	48.0	37.7(7)	1.93	72.8(13)	
$\langle {}^{10}\mathrm{C}\|{}^{9}\mathrm{C}+n\rangle$							
SM	1.06	0.70	91.1	24.8	1.93	48.0	
NCSM	1.51(2)	0.79(2)	61.6	28.6(6)	1.52	43.4(9)	23.2(10)
VMC	1.38(4)	1.14(6)	70.9	29.5(6)	1.04	30.8(6)	

observations. For simplicity, the following discussion is therefore restricted to 120 MeV/u and ^{9}Be targets but the conclusions would be identical for the alternative set of experimental conditions. Theoretical cross sections in Table II were obtained from the product of the single-particle cross sections and the spectroscopic factors calculated using the Cohen-Kurath POT interaction [27] and were increased by an additional $A/(A-1)$ center-of-mass motion correction of 1.11 as described in Ref. [14]. This conventional approach overpredicts the experimental cross sections and is consistent with the systematics of Ref. [16].

For light nuclei one is not limited to shell-model and mean-field derived inputs but can instead use densities and overlaps from VMC and NCSM calculations. In this work, VMC calculations were performed using a Hamiltonian constructed from the Argonne v_{18} [28] and Urbana IX [29] 2- and 3-body interactions, respectively. The NCSM calculations utilized the CD-Bonn 2000 [30] NN interaction with a $12\hbar\Omega$ harmonic-oscillator (HO) basis space and frequency $\hbar\Omega = 9$ MeV. Projectile-residue overlaps obtained from both calculations are shown in Fig. 2. For consistency, these overlaps were also fit with the Woods-Saxon parametrization. Although their shapes differ qualitatively at large radii the majority of the overlap lies below $r = 5$ fm and is well described by the fit. Plotting the integrated square of the overlap (insets of Fig. 2) highlights the dominant contribution below $r = 5$ fm where the VMC and NCSM also agree qualitatively on the shapes of the overlaps. The difference between them is primarily a scale factor. Woods-Saxon fit parameters r and a and the spectroscopic factors derived from each of these models are listed in Table II. The ~0.7 mb uncertainty in the single-particle cross sections represents the spread in calculated results when the radius parameter r is varied between $\pm 1\sigma$. The point nucleon densities generated from the VMC and NCSM calculations were also used as input into the calculations of the $A = 9$ core-target S matrices. Single-particle cross sections obtained using VMC and NCSM are provided in Table II. Although the radius parameters derived from the Woods-Saxon fits to the overlaps differ by ~10% between VMC and NCSM, these differences, and those in the calculated densities nevertheless result in similar single-particle cross sections.

Quantitatively, the fundamental difference between the theoretical cross sections arises from differences in the spectroscopic factors derived from each model. Compared to the experimental cross section of 73(4) mb for neutron knockout from ^{10}Be, the VMC result 72.8 (13) mb is in excellent agreement while the NCSM value 86.9(16) mb is ~20% larger. This discrepancy could arise from a number of sources including the differences in the descriptions of the nuclear size and continuum effects near the Fermi surface due to the distinct bases of the

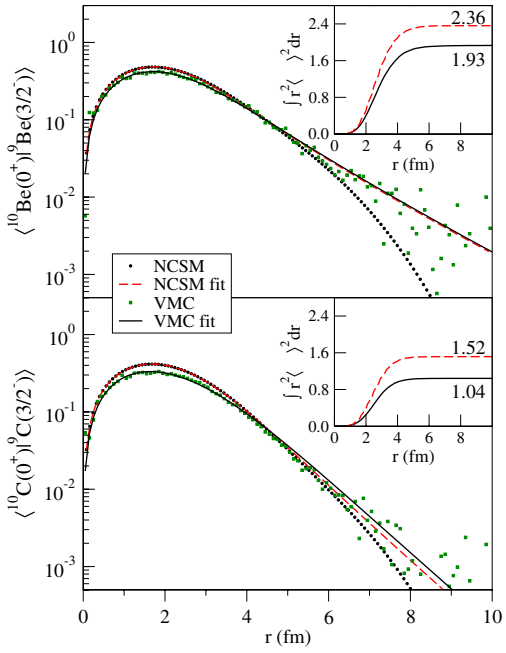

FIG. 2 (color online). Bound-state VMC and NCSM wave function overlaps and resulting fits that use a Woods-Saxon-plus-spin-orbit potential. (Inset) Integrals of the square overlaps that saturate at the theoretical spectroscopic factor.

calculations. The influence of 3-body forces, included in the VMC calculations, may also play a role. The agreement between experiment and VMC demonstrates the sensitivity of these reactions for providing a possible means to discriminate between *ab initio* structure models and suggests a new observable that can constrain their development.

For neutron knockout from ^{10}C, the NCSM cross section 43.4(9) mb is nearly twice as large as the 23.2(10) mb observed experimentally. The 30.8(6) mb calculated with VMC offers an improvement but is ~30% larger than the experimental result. This level of agreement likely reflects the accuracy in applying the eikonal model, specifically the underlying assumption that the $A = 9$ cores are spectators to the removal mechanism, to such an extreme case of deeply bound neutrons. The discrepancy between VMC and NCSM spectroscopic factors increases from 20% in $\langle^{10}\mathrm{Be}|^{9}\mathrm{Be} + n\rangle$ to nearly 50% for $\langle^{10}\mathrm{C}|^{9}\mathrm{C} + n\rangle$ indicating that continuum effects, neglected in the NCSM, may also play an important role. This will be investigated in the future with the NCSM/RGM formalism [31].

In summary, cross sections have been determined following single neutron knockout reactions from ^{10}Be and ^{10}C at intermediate energy. Point nucleon densities and bound-state overlaps from VMC and NCSM calculations were included into the theoretical description of the knockout reaction mechanism. Comparisons of the experimental cross sections to those predicted theoretically demonstrate good agreement for the case of VMC calculations that include 2- and 3-body forces. Compared to VMC, the NCSM results calculated with the CD-Bonn 2-body interaction were between 20% and 50% larger for neutron knockout from ^{10}Be and ^{10}C, respectively. These comparisons demonstrate the sensitivity of knockout reactions to the overlaps generated by *ab initio* calculations. Further improvements to these emerging theoretical descriptions will benefit from the application of this technique to several additional *p*-shell nuclei.

The authors would like to acknowledge the insight and stimulus contributed by the late Professor Gregers Hansen to the proposal for this study. This work was supported by the National Science Foundation under Grants No. PHY-0606007 and No. PHY-0758099, the United Kingdom Science and Technology Facilities Council (STFC) under Grant No. ST/F012012, the U.S. Department of Energy Office of Nuclear Physics under Contract No. DE-AC02-06CH11357 and SciDAC Grant No. DE-FC02-07ER41457, and by LLNL under Contract No. DE-AC52-07NA27344. G. F. G. acknowledges financial support from the Natural Sciences and Engineering Research Council of Canada (NSERC).

*Present address: Grand Accélérateur National d'Ions Lourds (GANIL), CEA/DSM-CNRS/IN2P3, Bvd Henri Becquerel, 14076 Caen, France.
grinyer@ganil.fr
†Present address: TRIUMF, 4004 Wesbrook Mall, Vancouver, British Columbia V6T 2A3, Canada.
‡Present address: CEA, Centre de Saclay, IRFU/Service de Physique Nucléaire, F-91191 Gif-sur-Yvette, France.

[1] S. C. Pieper and R. B. Wiringa, Annu. Rev. Nucl. Part. Sci. **51**, 53 (2001).
[2] P. Navrátil, S. Quaglioni, I. Stetcu, and B. R. Barrett, J. Phys. G **36**, 083101 (2009).
[3] P. Mueller *et al.*, Phys. Rev. Lett. **99**, 252501 (2007).
[4] L. Lapikás, J. Wesseling, and R. B. Wiringa, Phys. Rev. Lett. **82**, 4404 (1999).
[5] A. H. Wuosmaa *et al.*, Phys. Rev. Lett. **94**, 082502 (2005).
[6] A. H. Wuosmaa *et al.*, Phys. Rev. C **78**, 041302(R) (2008).
[7] E. A. McCutchan *et al.*, Phys. Rev. Lett. **103**, 192501 (2009).
[8] T. Aumann *et al.*, Phys. Rev. Lett. **84**, 35 (2000).
[9] V. Guimarães *et al.*, Phys. Rev. C **61**, 064609 (2000).
[10] A. Navin *et al.*, Phys. Rev. Lett. **85**, 266 (2000).
[11] V. Maddalena *et al.*, Phys. Rev. C **63**, 024613 (2001).
[12] B. A. Brown, P. G. Hansen, B. M. Sherrill, and J. A. Tostevin, Phys. Rev. C **65**, 061601 (2002).
[13] J. Enders *et al.*, Phys. Rev. C **67**, 064301 (2003).
[14] P. G. Hansen and J. A. Tostevin, Annu. Rev. Nucl. Part. Sci. **53**, 219 (2003).
[15] D. Bazin *et al.*, Phys. Rev. Lett. **91**, 012501 (2003).
[16] A. Gade *et al.*, Phys. Rev. C **77**, 044306 (2008).
[17] A. Gade and T. Glasmacher, Prog. Part. Nucl. Phys. **60**, 161 (2008).
[18] D. J. Morrissey, B. M. Sherrill, M. Steiner, A. Stolz, and I. Wiedenhoever, Nucl. Instrum. Methods Phys. Res., Sect. B **204**, 90 (2003).
[19] D. Bazin, J. A. Caggiano, B. M. Sherrill, J. Yurkon, and A. Zeller, Nucl. Instrum. Methods Phys. Res., Sect. B **204**, 629 (2003).
[20] M. Berz, K. Joh, J. A. Nolen, B. M. Sherrill, and A. F. Zeller, Phys. Rev. C **47**, 537 (1993).
[21] C. A. Bertulani and P. G. Hansen, Phys. Rev. C **70**, 034609 (2004).
[22] A. Gade *et al.*, Phys. Rev. C **71**, 051301 (2005).
[23] S. McDaniel *et al.*, Phys. Rev. C **81**, 024301 (2010).
[24] J. A. Tostevin, J. Phys. G **25**, 735 (1999).
[25] J. A. Tostevin, Nucl. Phys. **A682**, 320c (2001).
[26] B. A. Brown, Phys. Rev. C **58**, 220 (1998).
[27] S. Cohen and D. Kurath, Nucl. Phys. **73**, 1 (1965).
[28] R. B. Wiringa, V. G. J. Stoks, and R. Schiavilla, Phys. Rev. C **51**, 38 (1995).
[29] B. S. Pudliner, V. R. Pandharipande, J. Carlson, and R. B. Wiringa, Phys. Rev. Lett. **74**, 4396 (1995).
[30] R. Machleidt, Phys. Rev. C **63**, 024001 (2001).
[31] S. Quaglioni and P. Navrátil, Phys. Rev. Lett. **101**, 092501 (2008).